Geoderma 440 (2023) 116730

Contents lists available at ScienceDirect

Geoderma

journal homepage: www.elsevier.com/locate/geoderma

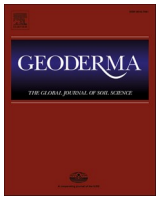

Demonstrating sorption analogy of lanthanides in environmental matrices for effective decision-making: The case of carbon-rich materials, clay minerals, and soils

Joan Serra-Ventura [a], Anna Rigol [a,b,*], Miquel Vidal [a]

[a] Department of Chemical Engineering and Analytical Chemistry, Faculty of Chemistry, Universitat de Barcelona, Martí i Franquès 1-11, 08028 Barcelona, Spain
[b] Institut de Recerca de l'Aigua (IdRA), Universitat de Barcelona, Martí i Franquès 1-11, 08028 Barcelona, Spain

ARTICLE INFO

Handling Editor: M. Tighe

Keywords:
Lanthanides
Sorption
Soil
Biochar
Activated charcoal
Clay mineral

ABSTRACT

Examining the effect of lanthanide-contaminated wastes, which have the potential to impact to other environmental compartments, requires conducting interaction studies with soils, as feasible first receptors of lanthanide leachates, and, if necessary, with sorbent materials, such as clay minerals and carbon-rich materials, which can serve as natural barriers and immobilisation agents used in remediation strategies. In this context, it is relevant to have available and reliable data on solid–liquid distribution coefficients (K_d) to understand the lanthanide sorption in these environmental matrices. Moreover, confirming lanthanide sorption analogies permits filling data gaps and data extrapolation among different contaminated scenarios, and thus facilitate to have available input data for decision-making related to the impact of a contaminated site. In this study, we demonstrate for the first time an analogous sorption of La, Sm, and Lu in carbon-rich materials (i.e., biochar and activated charcoal), clay minerals and soils, through laboratory batch experiments. The obtained sorption K_d values revealed similar sorption patterns among the three lanthanides for each matrix tested, even at different initial lanthanide concentrations. In all matrices, the maximum K_d values exceeded 10^4 L kg^{-1}, with a significant decrease when testing high lanthanide concentrations. The analogy was first confirmed by examining the K_d correlations for the La-Sm, Lu-Sm, and La-Lu pairs within each matrix, for which strong linear correlations were obtained in all cases. Data compilations were built with own and literature data, and derived cumulative distribution functions revealed statistically equal lanthanide distributions and K_d best estimates. In addition to this, K_d variability decreased when grouping the data according to significant material properties. For the first time, K_d (Ln) best-estimates for different scenarios and materials were proposed as input data for risk assessment models.

1. Introduction

Lanthanides (Ln) are widely used in technological sectors, with magnets, catalysts, and alloys forming the largest commercial markets (Eliseeva and Bünzli, 2011; Navarro and Zhao, 2014; Stegen, 2015). Their growing use is causing a related increase in Ln-enriched wastes and source-terms that could affect environmental compartments. Soil and aquatic systems with concerning levels of Ln are increasingly found all around, especially in China, a worldwide major producer and supplier (da Pereira et al., 2022; Sthiannopkao and Wong, 2013), but also in other mine-influenced waters in sites around the world (Gomes et al., 2022; Verplanck et al., 2004). Li and Wu (2017) reported up to 100, 70, and 3 μg L^{-1} of lanthanum (La), samarium (Sm), and lutetium (Lu), respectively, and Sun et al. (2012) reported up to 80, 30, and 1 μg L^{-1} of La, Sm, and Lu, respectively, in Chinese rivers affected by acid mine drainage. In Europe, unusual enrichments of lanthanides in water bodies of the Wiśniówka mining area have been reported, with concentrations up to 2600, 1900, and 120 μg L^{-1} of La, Sm, and Lu, respectively (Migaszewski et al., 2019), and approximately 1800, 610, and 8 μg L^{-1} of La, Sm, and Lu, respectively, in acidic waters of Tinto River, in Spain (Lecomte et al., 2017). Monitoring Ln concentrations in environmental compartments and examining the interaction of waste-leached Ln in soils, which are a key environmental compartment governing pollutant fate, are key steps in assessing the risk derived from the increase in Ln

* Corresponding author at: Department of Chemical Engineering and Analytical Chemistry, Faculty of Chemistry, Universitat de Barcelona, Martí i Franquès 1-11, 08028 Barcelona, Spain.
E-mail address: annarigol@ub.edu (A. Rigol).

https://doi.org/10.1016/j.geoderma.2023.116730
Received 1 August 2023; Received in revised form 9 October 2023; Accepted 27 November 2023
Available online 5 December 2023

wastes. It is reported that a long-term exposure to these wastes can cause adverse effects in human health related with DNA damage or cell death (Brouziotis et al., 2022).

The interaction of Ln in soils depends on their edaphic properties and the relative weight of the phases such as organic matter, clay minerals, and metal oxides (Ramírez-Guinart et al., 2017). To lower the mobility of Ln in soils or remove them from aqueous systems, different types of materials are increasingly being applied. Among these, clay minerals have been used as soil amendments to decrease radionuclide mobility in soils (Vidal et al., 2001) and are often used as engineered barriers in the management of nuclear wastes rich in Ln and actinides (Alba et al., 2011). Carbon-rich materials such as activated charcoal are one of the most commonly used sorbents, as they have high sorption capacities due to their high specific surface area and microporous systems (Tan et al., 2015). An alternative attracting increasing interest is biochar, a carbon-rich material derived from biomass residues pyrolysed in the absence of oxygen, thus permitting the implementation of a circular economy for soil and water treatment (Saravanan and Kumar, 2022). By optimising the pyrolysis procedure, a wide range of the physicochemical properties of biochar can be improved such as surface functionalisation, exchange capacity, and surface area (Gopinath et al., 2021), enabling an increase in their sorption capacity. Other carbon-rich materials that could be used for the same purpose are coal fines, a by-product of coal originating from metallurgic industries that has a low market value and usually accumulates in stockpiles due to its expensive disposal.

To investigate the sorption behaviour of Ln in carbon-rich materials, clay minerals, and soils, laboratory methods such as batch sorption experiments are required to derive sorption parameters as the solid–liquid distribution coefficient (K_d, L kg^{-1}) (Aldaba et al., 2010; Ramírez-Guinart et al., 2017). However, sorption data of Ln in environmental matrices currently available in the literature do not permit to demonstrate or discard a comparable behaviour of Ln for the same type of pure soil phase, bulk soil or an environmentally relevant material. This makes it difficult to understand the Ln sorption process and to extrapolate existing information to untested Ln. For this reason, the present work investigated the possible chemical analogies in the sorption of Ln in different matrices of environmental interest by obtaining data from batch experiments and enhancing the resulting datasets with data available in the literature. La, Sm, and Lu were used as representatives of the Ln series, since La and Lu present the most different ionic radii, while the existence of both stable and radioactive isotopes makes Sm a lanthanide of interest to be examined. Carbon-rich materials, clay minerals, and soils were selected as the environmental matrices under study, and their K_d values and distribution functions were compared to examine similarities or differences in their Ln sorption pattern. This analysis allowed us to identify the relevant factors affecting the variability of Ln sorption and provide modellers with a single K_d (Ln) best-estimate for each material.

2. Materials and methods

2.1. Samples and sample characterisation

The carbon-rich materials used in this work were classified into three groups: biochars, coal fines, and activated charcoals. The four biochars tested were produced by slow pyrolysis at 350 °C in the absence of oxygen and came from different feedstocks: castor meal (CM), eucalyptus forest residues (CE), sugarcane bagasse (SB), and the pericarp of green coconut (PC). The samples were sieved to obtain a particle size of < 2 mm. The coal fines (CF) were from the waste of a metallurgical industry. The two activated charcoals, an untreated (GAC) and a steam-activated one for water processing (NGAC), were supplied by Merck. The characterisation data of the carbon-rich materials used are summarised in Section S1 and Table S1 in the Supplementary Material.

Four natural smectite clays (2:1 phyllosilicates) were used in this work: a hectorite (HEC) (Source Clays Repository of the Clay Minerals Society, University of Missouri, Columbia, USA), two montmorillonites (STx-1 (Source Clays Repository of the Clay Minerals Society, University of Missouri, Columbia, USA), and SCa-3 (Solvay Alkali GMBH)); and a bentonite (FEBEX) (ENRESA, Spain), with a montmorillonite content greater than 90 % (Villar et al., 1998). Only the fraction of < 2 μm was used for the sorption experiments. The characterisation data of the clay minerals used are summarised in Section S1 and Table S2 in the Supplementary Material.

Six agricultural soil samples from Spain and other locations across Europe (DELTA2, DUBLIN, ANDCOR, CABRIL, ASCO, and RED STONE) with contrasting edaphic properties were selected from a well-characterised collection of soils (Ramírez-Guinart et al., 2017). All soil samples were taken from the surface layer (0–10 cm), air-dried and sieved to obtain a particle size of < 2 mm. The classification and characterisation data of the soils used are summarised in Section S1 and Table S3 in the Supplementary Material.

2.2. Laboratory batch sorption experiments

The sorption experiments consisted of equilibrating 2 g of carbon-rich materials, 0.2 g of clay samples, and 1 g of soils with 50, 30, and 25 mL of the initial Ln solutions, respectively, in polypropylene centrifuge tubes. La, Sm, and Lu stock solutions were prepared by dissolving weighed amounts of $La(NO_3)_3$, $Sm(NO_3)_3$, and $Lu(NO)_3$ (Merck), respectively. Dilutions were performed to obtain the Ln solutions within the range of 0.03 to 10/13 meq L^{-1}, which defined Ln initial concentrations. These concentrations are representative for environmental polluted scenarios due to mine leachates, as earlier mentioned, while the highest initial concentration served to quantify the maximum sorption capacity of the materials. The suspensions were placed in an end-over-end shaker for 24 h, an adequate contact time to reach equilibrium in the three matrices tested in this study (Coppin et al., 2002; Kołodyńska et al., 2018; Ladonin, 2019). The samples were then centrifuged at 4400 g for 15 min in a Hettich Rotina 420 centrifuge. The supernatants obtained were decanted, filtered through 0.45-μm nylon syringe filters, and stored in polyethylene vials at 4 °C. Aliquots for the analysis of La, Sm, and Lu were acidified to 1 % HNO_3. The same procedure was followed for the blank experiments, without spiking with the Ln solutions. Supernatant aliquots from the blank sorption experiments were used to obtain the characterisation parameters mentioned in Section S1 of the Supplementary Material.

2.3. Analytical measurements

The levels of La, Sm, Lu, as well as of the major cations Ca, Mg, K, and Na, in the solutions from the sorption experiments were determined by inductively coupled plasma optical emission spectroscopy (ICP-OES) using a PerkinElmer Optima 3200 RL spectrometer (Perkin Elmer) and the following emission lines (in nm): La, 408.672; Sm, 359.260; Lu, 261.542; Ca, 317.933; Mg, 279.077; K, 766.490; and Na, 589.592. In the cases where the concentrations were below the quantification limit for ICP-OES (Lu, Ca, and Mg: 0.05 mg L^{-1}; La and Sm: 0.1 mg L^{-1}; and K and Ca: 0.5 mg L^{-1}), the concentrations were determined by inductively coupled plasma mass spectrometry (ICP-MS) using a PerkinElmer ELAN 6000 spectrometer. The limits of quantification for ICP-MS were 0.1 μg/L for La and Sm, and 0.5 μg/L for Lu.

2.4. Data treatment

The sorbed Ln concentration (C_{sorb}, mg kg^{-1}) was calculated from the initial (C_i, mg L^{-1}) and equilibrium (C_{eq}, mg L^{-1}) Ln concentrations using the following equation (Eq. (1)):

$$C_{sorb} = \left(C_i - C_{eq}\right) * V/m \quad (1)$$

where m is the mass of material (carbon-rich material, soil or clay

mineral) used in the experiment (kg) and V the volume of the initial Ln solution added (L).

The sorption solid–liquid distribution coefficient (K_d, L kg^{-1}) was calculated as the ratio of the target Ln C_{sorb} and C_{eq}, as follows (Eq. (2):

$$K_d = C_{sorb}/C_{eq} \quad (2)$$

2.5. Creation of the K_d (Ln) datasets

The K_d values of the three Ln in the different matrices obtained in this work by sorption batch experiments were combined with the data compiled from the literature after a critical review of the available data and publications. The terms used during the search were: 'rare earth elements', 'lanthanides', 'lanthanum', 'samarium', 'lutetium' and/or 'biochar', 'activated charcoal', 'soil', 'clay mineral' and/or 'sorption', 'adsorption', and 'removal', among other combinations. The K_d values from the literature were only accepted if they were directly reported in the body of the manuscript or could be easily extracted from the figures. Furthermore, they had to be derived from batch sorption experiments. Thus, the gathered K_d data were obtained through single-point K_d, linear sorption isotherms and the linear part of Langmuir-shaped sorption isotherms. The overall datasets, comprising our experimental data and the data from the literature, consisted of 35 entries for La, 33 for Sm, and 28 for Lu in carbon-rich materials; 70 entries for each Ln in clay minerals; and 44 entries for La and 42 each for Sm and Lu in soils. The references used and the entries extracted for the K_d datasets of La, Sm, and Lu in the three matrices, along with the sorption data from this work, are shown in Table S4 in the Supplementary Material.

2.6. Statistical analysis of the K_d (Ln) datasets

The K_d datasets of each matrix tested were subjected to linear regressions using the least-squares method (MATLAB R2022a, MathWorks, Inc.) to assess the relationship between the La-Sm, Lu-Sm, and La-Lu K_d pairs.

The chemical equilibrium diagrams of Ln in specific scenarios were constructed using the Chemical Diagrams Medusa-Hydra software.

The K_d parameter is $\log_{10}$-normally distributed (Ramírez-Guinart et al., 2020; Sheppard, 2011). Therefore, it only takes positive real values. Thus, a log K_d distribution can be described by means of the location parameters of percentiles (the 50th percentile, which is considered the most probable value of the distribution (the so-called K_d best estimate, BE), and the 5th and 95th percentiles) and the scale parameter (or geometrical standard deviation, GSD) that estimates the log K_d variability within a dataset. First, the log K_d values of a certain dataset were ordered by increasing value and given an empirical frequency equal to 1/n, where n is the number of entries in the dataset. Then, the experimental cumulative distribution functions (CDF) were derived by assigning a cumulative frequency to the sorted log K_d values, which is the sum of the preceding frequencies (up to 1). The resulting CDF was subjected to the Kolmogorov-Smirnov test to ensure it followed a normal distribution and fitted to the theoretical CDF equation using the least-squares method through the cftool toolbox of MATLAB. The fitted CDF allowed us to obtain the BE from the 50th percentile antilog and the GSD from the standard deviation antilog. The Fisher's least significant difference (FLSD) test used for pairwise comparisons of the $\log_{10}$-transformed K_d datasets was performed with Statgraphics Centurion 18 (Statgraphics Technologies, Inc.). To obtain more valuable K_d BE with a lower associated variability, the datasets were refined by following different criteria for each of the matrix tested and splitting them into partial datasets, ensuring a sufficient number of entries to obtain CDFs with an appropriate goodness-of-fit.

3. Results and discussion

3.1. Examination of the Ln sorption analogy in carbon-rich materials

3.1.1. Description of Ln sorption in carbon-rich materials

Table 1 summarises the derived K_d values of La, Sm, and Lu from our own experiments, with the initial Ln concentration indicated for each experiment, and Table S5 in Supplementary Material summarises the equilibrium concentrations of each experiment. Within each carbon-rich material, La, Sm, and Lu generally showed the same trend when increasing the initial concentration. In the case of biochars, as previously observed for Sm (Serra-Ventura et al., 2022), the maximum K_d values of La and Lu were not mostly found at the lowest concentration tested (0.05 meq L^{-1}), but at the next higher initial concentration. A further increase in the initial concentration led to a decrease in the K_d values due to saturation of the sorption sites. Still, the sorption process of La and Lu in biochars at the lowest initial concentrations could be hampered by competition with solution components such as dissolved organic carbon (DOC), which could prevent the Ln from binding to the carbon-rich material by forming soluble chelates with it (see Table S1 in the Supplementary Material). To support this, chemical equilibrium diagrams were obtained at different initial Ln concentrations and with varying DOC contents of the materials. Given the difficulty of modelling DOC-Ln complexation and considering that the major fraction of DOC is primarily composed of carboxylic groups and, to a lesser extent, phenolic groups the complexing capacity of DOC was simulated using ethylenediaminetetraacetic acid (EDTA) as a proxy. The diagrams in Fig. S1 of the Supplementary Material show an equally distributed presence of the $Ln(EDTA)^-$ and Ln(HEDTA) species, in addition to the free Ln ion and cationic species, at the initial and final experimental pH, proving a similar speciation and the same effect of DOC for the three Ln.

Regarding coal fines and activated charcoals, the three Ln presented a huge affinity for the matrix (near or higher than 10^5 L kg^{-1}), which was much higher than that for biochars. However, whereas low K_d values at high initial concentrations were not observed in CF and GAC, 10 meq L^{-1} of La, Sm or Lu was enough to saturate the sorption sites in

Table 1
Sorption data for the three Ln tested at different initial concentrations in carbon-rich materials (C_i in meq L^{-1} and K_d in L kg^{-1}).

Sample	C_i	K_d (La)	K_d (Sm)	K_d (Lu)
CM	0.05	4200	2790	1310
	0.1	11,500	2820[a]	2650
	3	16,600	14,100[a]	2250
	10	117	123[a]	91
CE	0.05	6900	5800	1640
	0.1	23,300	1780[a]	574
	3	45	27	28
	10	6.0	16[a]	7.5
PC	0.05	560	550	520
	0.1	7720	1660[a]	435
	3	228	227	162
	10	11	31[a]	13
SB	0.05	2140	1650	880
	0.1	3650	135[a]	611
	3	31	22[a]	14
	10	4.0	2.3[a]	4.5
CF	0.05	573	457	620
	0.1	8990	1600[a]	1710
	3	81,300	64,600[a]	56,400
	10	73,300	85,300[a]	54,300
GAC	0.05	16,000	15,000	9000
	0.1	40,900	26,000[a]	6300
	3	35,200	144,000[a]	62,500
	10	1,070,000	64,600[a]	192,000
NGAC	0.05	200,000	197,000	130,000
	0.1	287,000	12,600[a]	16,400
	3	128,000	51,600[a]	96,600
	10	42	44[a]	53

[a] K_d data from Serra-Ventura et al. (2022).

NGAC. Therefore, these results were the first indication that factors such as the Ln concentration or the nature of the carbon-rich material are more relevant in Ln sorption than the specific Ln involved in the sorption process.

3.1.2. Examination of the compiled K_d (Ln) data and CDFs in carbon-rich materials

The bibliographic research identified several relevant studies involving biochars and chemically activated biochars, with entries concerning batch sorption experiments with La and Sm that were accepted into the overall dataset (Awwad et al., 2010; Chen, 2010; Hadjittofi et al., 2016; Wang et al., 2016; Liatsou et al., 2017; Kołodyńska et al., 2018; Zhao et al., 2021), along with our sorption data shown in Table 1.

To examine Ln analogy within the group of the carbon-rich materials, linear regression analyses were performed within the overall dataset between K_d data of the La-Sm, Lu-Sm, and La-Lu pairs, when available for the same material. As the literature data did not present any of these pairs, linear regressions were performed only with our sorption K_d data. Significant linear correlations with the three pairs of $\log_{10}$-transformed K_d data were found (p-value < 0.05), presenting the following equations, with the confidence range in brackets. Graphical representations of these correlations are provided in Fig. S2 in the Supplementary Material.

$\log K_d$ (Sm) = 0.8 (0.1) x $\log K_d$ (La); N = 28, $R^2 = 0.91$

$\log K_d$ (Sm) = 1.0 (0.1) x $\log K_d$ (Lu); N = 28, $R^2 = 0.94$

$\log K_d$ (Lu) = 0.8 (0.1) x $\log K_d$ (La); N = 28, $R^2 = 0.92$

The correlations presented a non-significant y-intercept, suggesting that there was not a relevant bias between the K_d of the two Ln tested. The slope obtained for Sm vs. Lu was statistically 1, indicating a direct analogy, while for the La-Sm and La-Lu pairs was also near to 1.

By arranging the data in terms of the CDF of the overall dataset, it was possible to evaluate and describe the variability in the K_d datasets of La, Sm, and Lu in carbon-rich materials (see Fig. 1). The probabilistic approach led to obtain K_d BE values with a difference of less than one order of magnitude between La and Lu (3040 and 970 L kg^{-1}, respectively), which were not statistically different. However, the CDF showed high variability due to the different nature of the carbon-rich materials included and the wide range of Ln concentrations that were compared. To reduce data variability, besides excluding the unlikely event of finding 10 meq L^{-1} of Ln in a natural waste leachate, a two-group split was tested. One group contained the biochars (CM, CE, PC, SB, and the literature entries), while the other contained the rest of the carbon-rich materials (CF, GAC, and NGAC). The grouping criterion resulted in K_d distributions with a lower intrinsic variability, with all the fitted CDFs presenting regression coefficients higher than 0.92. The K_d BE values obtained for the non-biochar carbon-rich materials were higher by more than one order of magnitude than those for the biochars, the first one being a more suitable option for remediation purposes. Within each group, the La, Sm, and Lu datasets and their K_d BE values were statistically equal according to the FLSD test, but statistically different when comparing the same Ln values between the two different groups. This was consistent with the previous examination of the sorption data, demonstrating that the three Ln presented a similar sorption behaviour in carbon-rich materials with different origins and characteristics. This observation led to the building of a joint La, Sm, and Lu dataset, considering that the data could be treated as lanthanides (Ln). Thus, two statistically different K_d best-estimates for Ln were proposed for biochars and other carbon-rich materials, differing in one order of magnitude.

3.2. Examination of the Ln sorption analogy in clay minerals

3.2.1. Description of Ln sorption in clay minerals

The K_d values obtained from the batch experiments with the clay minerals at differing C_i are summarised in Table 2, whereas Table S6 in Supplementary Material reports the experimental C_{eq} measured.

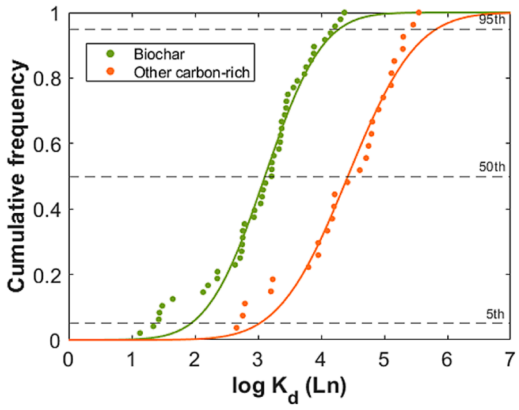

Material	Dataset	N	BE	PCTL 5	PCTL 95	GSD
Overall	La	35	3040	13	$> 10^5$	28
	Sm	33	1730	3.2	$> 10^5$	21
	Lu	28	970	4.1	$> 10^5$	28
Biochar[a]	La	19	2040	98	42665	6.3
	Sm	17	1400	140	14000	4.1
	Lu	12	550	83	3660	3.2
	Ln	**48**	**1290**	**86**	**19300**	**5.2**
Other carbon-rich[a]	La	9	44360	2120	$> 10^5$	6.4
	Sm	9	18110	760	$> 10^5$	6.9
	Lu	9	11980	400	$> 10^5$	7.9
	Ln	**27**	**26530**	**1050**	**$> 10^5$**	**7.1**

Fig. 1. CDFs for Ln and the parameters of the CDFs for La, Sm, Lu, and Ln (BE, PCTL 5, PCTL 95, and GSD: L kg^{-1}) in the overall and partial datasets of biochars and other carbon-rich materials. [a]Data obtained at initial Ln concentration of 10 meq L^{-1} were excluded.

Table 2
Sorption data for the three Ln tested at different initial concentrations in clay minerals (C_i in meq L^{-1} and K_d in L kg^{-1}).

Sample	C_i	K_d (La)	K_d (Sm)	K_d (Lu)
HEC	0.03	43,820	15,765	14,010
	0.3	33,370[a]	65,240	27,900
	3	25,140[a]	22,590	15,270
	13	76[a]	78	102[a]
SCa-3	0.03	33,100[a]	19,100	48,500[a]
	0.3	17,900[a]	14,600	15,800
	3	12,800[a]	54,200	26,700[a]
	13	238[a]	180	203[a]
STx-1	0.03	18,000[a]	4970	15,600[a]
	0.3	13,200[a]	27,300	12,400[a]
	3	11,100[a]	9310	11,300[a]
	13	99[a]	87	100[a]
FEBEX	0.03	23,800[a]	12,100	32,900[a]
	0.3	19,100[a]	29,900	31,500[a]
	3	15,200[a]	22,800	15,300[a]
	13	106[a]	133	171[a]

[a] K_d data from Galunin et al. (2010).

K_d data revealed a similar sorption pattern among the three different Ln studied. As in previous studies, a Langmuir behaviour was observed in all cases. All the 2:1 phyllosilicates presented high K_d values until the saturation of the sorption sites at the maximum initial concentration tested (Galunin et al., 2010). The K_d values obtained were higher than 10^4 L kg^{-1} in all cases, revealing a strong and durable affinity across the different initial concentrations tested. This affinity could be associated with the formation of inner-sphere complexes between Ln and the clay

surface as it was previously reported in literature (Stumpf et al., 2002; Hartmann et al., 2008), in which the complexes were favoured by the basic nature and low ionic strength of the contact solution. In most cases, the sorption for the low initial concentration range followed a linear trend.

3.2.2. Examination of the compiled K_d (Ln) data and CDFs in clay minerals

The gathering of the batch sorption data of Ln in clay minerals from the literature resulted in the finding of a few publications, some of which did not directly report the data in the body of the manuscript (Gu et al., 2022). The collected K_d data came from two scientific publications, producing 54 new entries for 1:1 and 2:1 clay minerals (kaolinite, smectite, and halloysite) under different experimental conditions of pH (from 3 to 7.5), ionic strength (0.01 and 0.025 M $NaNO_3$), and initial Ln concentration (100 to 130 μg/L), among others (Coppin et al., 2002; Yang et al., 2019). The selection of K_d data from these publications was made based on the representativeness of the laboratory conditions of environmental scenarios.

To examine Ln analogy within the group of clay minerals, linear regression analyses were performed using the overall dataset. For this type of material, all the accepted literature entries provided K_d data of the three Ln. Significant linear correlations with the three pairs of $\log_{10}$-transformed K_d data were found (p-value < 0.05), presenting the following equations, with the confidence range in brackets (see graphical representations in Fig. S3 in the Supplementary Material):

$\log K_d$ (Sm) = 1.04 (0.06) x $\log K_d$ (La); N = 70, $R^2 = 0.94$

$\log K_d$ (Sm) = 0.95 (0.04) x $\log K_d$ (Lu); N = 70, $R^2 = 0.96$

$\log K_d$ (Lu) = 1.07 (0.07) x $\log K_d$ (La); N = 70, $R^2 = 0.94$

The correlations presented a non-significant y-intercept, suggesting that there was no relevant bias in any of the pairs examined. The slopes obtained were mostly statistically equal to 1, indicating a direct analogy among Ln and that the change of aqueous solution parameters, such as pH and ionic strength, equally affected the K_d values of La, Sm, and Lu.

The construction of the CDF of La, Sm, and Lu from the overall data gathered led to obtaining K_d BE values that were not statistically different according to the FLSD test (Fig. 2). Nevertheless, the clay minerals were grouped as 1:1 and 2:1 clay minerals to reduce the dataset variability, removing, as in the case of the carbon-rich materials, the data involving an initial concentration of 13 meq L^{-1}. As summarised in Fig. 2, the K_d BE values for the 1:1 clay minerals were lower by one order of magnitude than those for the 2:1 clay minerals, which is in agreement with previously published studies on the sorption of heavy metals in clays with different characteristics (Uddin, 2017).

Within each partial dataset, the K_d distributions of La, Sm, and Lu exhibited lower variability than that of the overall dataset, and regression coefficients greater than 0.98, with their BE values and distributions statistically equal according to the FLSD test. This confirmed the previous finding that changes in experimental conditions equally affected the K_d values of La, Sm, and Lu in both 1:1 and 2:1 clay minerals. As performed in the previous section, a joint La, Sm, and Lu dataset was built and two single and statistically different K_d (Ln) BE were proposed for both 1:1 and 2:1 clay minerals, differing by an order of magnitude. Thus, 2:1 clay minerals may be a more effective barrier in a remediation strategy.

3.3. Examination of the Ln sorption analogy in soils

3.3.1. Description of Ln sorption in soils

As seen in Table 3, La and Lu underwent similar sorption processes as the ones observed for Sm in a previously published work (Ramírez-Guinart et al., 2018), either exhibiting a linear K_d behaviour across the whole range of initial concentrations tested (DELTA2 and DUBLIN) or reaching site saturation at the highest initial Ln concentration of 10 meq L^{-1} (ANDCOR, CABRIL, ASCO, and RED STONE). Additionally, the equilibrium concentrations for the low initial Ln concentrations were predominantly within the range of 0.2 to 1000 μg L^{-1} for La, Sm, and Lu

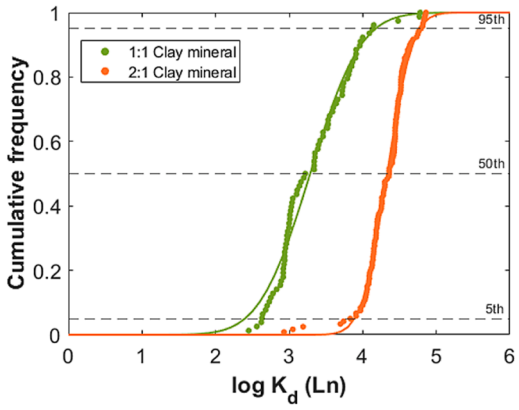

Material	Dataset	N	BE	PCTL 5	PCTL 95	GSD
Overall	La	70	7540	540	$> 10^5$	5.0
	Sm	70	8215	440	$> 10^5$	6.0
	Lu	70	8700	370	$> 10^5$	6.8
1:1 Clay mineral[a]	La	26	1930	270	13855	3.3
	Sm	26	1850	250	13820	3.4
	Lu	26	1725	210	14230	3.6
	Ln	**78**	**1930**	**250**	**14900**	**3.5**
2:1 Clay mineral[a]	La	40	18120	6750	48620	1.8
	Sm	40	21940	8030	59980	1.8
	Lu	40	24000	8220	70050	1.9
	Ln	**120**	**21500**	**7750**	**59500**	**1.9**

Fig. 2. CDFs for Ln and the parameters of the CDFs for La, Sm, Lu, and Ln (BE, PCTL 5, PCTL 95, and GSD: L kg^{-1}) in the overall partial datasets of 1:1 and 2:1 clay minerals. [a]Data obtained at initial Ln concentration of 13 meq L^{-1} were excluded.

Table 3
Sorption data for the three Ln tested at different initial concentrations in soils (C_i in meq L^{-1} and K_d in L kg^{-1}).

Sample	C_i	K_d (La)	K_d (Sm)	K_d (Lu)
DELTA2	0.05	21,000	17,800	5900
	0.1	22,900	16,100[a]	6300
	3	20,000	18,600[a]	10,300
	10	64,700	22,500[a]	10,900
DUBLIN	0.05	2710	2510[a]	1130
	0.1	2460	2500	1180
	3	3100	2870[a]	1530
	10	7320	4870	2290
ANDCOR	0.05	1690	1350[a]	510
	0.1	1830	1430[a]	534
	3	271	435[a]	345
	10	17	26[a]	19
CABRIL	0.05	9390	5300[a]	4980
	0.1	9410	6010	4120
	3	4380	6050[a]	1580
	10	25	29[a]	26
ASCO	0.05	78,300	297,000[a]	74,800
	0.1	94,100	95,500	56,700
	3	18,000	337[a]	834
	10	53	21[a]	30
RED STONE	0.05	1060	573	263
	0.1	1100	619	287
	3	382	410	210
	10	25	42	23

[a] K_d data from Ramírez-Guinart et al. (2018).

(see Table S7 in Supplementary Material).

To strengthen this assumption, Ln speciation in three different soils was investigated (see Fig. S4 in the Supplementary Material). The

speciation of the three Ln in the supernatant under conditions of varying pH and anions in solution was observed for high carbonate and sulphate levels in solution (ASCO), low carbonate and sulphate levels in solution (RED STONE), and high carbonate but low sulphate levels in solution (DUBLIN). In all cases, the predominant species in the range of pH values tested were very similar, with Ln^{3+}, $LnSO_4^+$, and $LnCO_3^+$ being the most predominant species. Hence, these same ones interact with the soil surface during the sorption process of La, Sm, and Lu.

3.3.2. *Examination of the compiled K_d (Ln) data and CDFs in soils*

In the bibliographic research of the K_d data for La, Sm, and Lu in soils, several publications were found, although a few of them did not directly report the data in the body of the manuscript or figures and they were not considered (Tang and Johannesson, 2005; Ladonin, 2019). Two scientific papers and two technical reports produced 21 new entries of the K_d values for La and 19 each for Sm and Lu in soils, tills, and gyttja (Dinali et al., 2019; Sheppard et al., 2009, 2011; Zuyi et al., 2000). The revision provided extra data for pH and salt conditions that were different to those used in our experiments, thus enriching the subsequent analysis of analogies between the Ln, but also increasing the related variability.

Significant linear correlations with the three pairs of log_{10}-transformed K_d data were found (p-value < 0.05), presenting the following equations, with the confidence range in brackets:

log K_d (Sm) = 0.98 (0.03) x log K_d (La); N = 43, $R^2 = 0.90$

log K_d (Sm) = 1.07 (0.02) x log K_d (Lu); N = 41, $R^2 = 0.97$

log K_d (Lu) = 0.92 (0.02) x log K_d (La); N = 43, $R^2 = 0.92$

The correlations presented a non-significant y-intercept, suggesting that there was not a relevant bias in any of the pairs examined, with slopes approaching to 1. Graphical representations are provided in Fig. S5 in the Supplementary Material.

The examination of the CDF of the overall datasets showed that the K_d BE values of the three Ln were within the same order of magnitude (see Fig. 3). The distributions were statistically equal according to the FLSD tests, but with high associated variability. A closer examination of the dataset led to the grouping of the data according to the dynamics of the interactions of the Ln with the soil. Therefore, 'freshly contaminated' (i.e., data from laboratory batch sorption experiments) and 'native' (i.e., data from desorption of soil native lanthanides, which actually led to the quantification of desorption K_d) data groups were created, excluding the 10 meq L^{-1} initial concentration K_d data. This approach reduced the variability of the partial datasets with respect to that of the overall dataset and enabled a better evaluation of the similarity of the Ln distributions in each group. The CDF of the partial datasets presented regression coefficients higher than 0.97.

The distributions of La, Sm, and Lu for freshly contaminated Ln were statistically different from those of La, Sm, and Lu for the native group, as confirmed by the FLSD test. Therefore, the management of long-term contaminated sites will be different to the one from freshly contaminated sites due to the interaction dynamics with the soil, hence requiring different decision-making. Within each group, statistically equal distributions of K_d BE values were obtained for the three Ln confirmed by the FLSD test. This suggested that La, Sm, and Lu behaved similarly in the short-term scenario of freshly contaminated soils as well as in the desorption of native Ln from the soil. Thus, a joint La, Sm, and Lu dataset was built in order to propose a single and statistically different K_d (Ln) BE for the two scenarios.

4. Conclusions

The systematic study with own and literature data of the sorption of La, Sm, and Lu in carbon-rich materials, clay minerals, and soils unequivocally showed a Ln sorption analogy in each of the group of materials tested. Splitting overall datasets into partial groups confirmed that the distributions of the three Ln tested were statistically equal when comparing carbon-rich materials with different characteristics (such as biochar versus activated charcoals and coal fines) and clay minerals with different structures (i.e., 1:1 and 2:1 phyllosilicates), as well as when the dynamics of the interaction between the Ln and soil were considered (i.e., freshly incorporated versus native Ln). The finding allowed us to simplify the analyses and create aggregated datasets where K_d data of La, Sm, and Lu were integrated, proposing single K_d (Ln) best-estimates for the risk assessment in the specific scenarios reported, which in turn contributes to filling gaps and enhance the knowledge for an eventual decision-making on the management of a contaminated site and the use of materials, such as the clays and carbon-rich materials here tested, for remediation purposes.

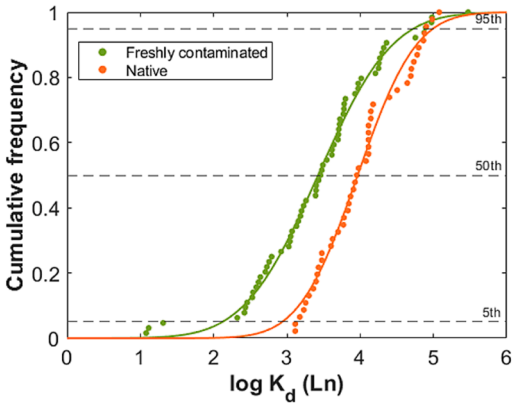

Material	Dataset	N	BE	PCTL 5	PCTL 95	GSD
Overall	La	44	5130	231	$> 10^5$	6.6
	Sm	42	4080	121	$> 10^5$	8.5
	Lu	42	2340	96	57310	7.0
Freshly contaminated[a]	La	22	3680	246	54970	5.2
	Sm	20	2530	101	63470	7.1
	Lu	22	1550	81	29450	6.0
	Ln	**64**	**2660**	**132**	**53500**	**6.2**
Native	La	16	10210	779	$> 10^5$	4.8
	Sm	16	9770	777	$> 10^5$	4.7
	Lu	14	6070	810	45430	3.4
	Ln	**46**	**9250**	**866**	**98800**	**4.2**

Fig. 3. CDF for Ln and parameters of the CDFs for La, Sm, Lu, and Ln (in L kg^{-1}) in the overall and the partial datasets of freshly contaminated and native Ln. [a]Data obtained at initial Ln concentration of 10 meq L^{-1} were excluded.

Declaration of competing interest

The authors declare that they have no known competing financial interests or personal relationships that could have appeared to influence the work reported in this paper.

Data availability

Data will be made available on request.

Acknowledgements

This work was carried out in a Generalitat de Catalunya Research Group (2021 SGR 01342) and has received funding from the Ministerio de Ciencia e Innovación de España (PID2020-114551RB-I00).

Appendix A. Supplementary data

Supplementary data to this article can be found online at https://doi.org/10.1016/j.geoderma.2023.116730.

References

Alba, M.D., Castro, M.A., Chaín, P., Hurtado, S., Orta, M.M., Pazos, M.C., Villa, M., 2011. Interaction of Eu-isotopes with saponite as a component of the engineered barrier. Appl. Clay Sci. 52 (3), 253–257. https://doi.org/10.1016/j.clay.2011.02.027.

Aldaba, D., Rigol, A., Vidal, M., 2010. Diffusion experiments for estimating radiocesium and radiostrontium sorption in unsaturated soils from Spain: Comparison with batch sorption data. J. Hazard. Mater. 181 (1–3), 1072–1079. https://doi.org/10.1016/j.jhazmat.2010.05.124.

Awwad, N.S., Gad, H.M.H., Ahmad, M.I., Aly, H.F., 2010. Sorption of lanthanum and erbium from aqueous solution by activated carbon prepared from rice husk. Colloids Surf. B Biointerfaces 81 (2), 593–599. https://doi.org/10.1016/j.colsurfb.2010.08.002.

Brouziotis, A.A., Giarra, A., Libralato, G., Pagano, G., Guida, M., Trifuoggi, M., 2022. Toxicity of rare earth elements: An overview on human health impact. Front. Environ. Sci. 10 (September), 1–14. https://doi.org/10.3389/fenvs.2022.948041.

Chen, Q., 2010. Study on the adsorption of lanthanum(III) from aqueous solution by bamboo charcoal. J. Rare Earths 28 (SUPPL. 1), 125–131. https://doi.org/10.1016/S1002-0721(10)60272-4.

Coppin, F., Berger, G., Bauer, A., Castet, S., Loubet, M., 2002. Sorption of lanthanides on smectite and kaolinite. Chem. Geol. 182 (1), 57–68. https://doi.org/10.1016/S0009-2541(01)00283-2.

Dinali, G.S., Root, R.A., Amistadi, M.K., Chorover, J., Lopes, G., Guilherme, L.R.G., 2019. Rare earth elements (REY) sorption on soils of contrasting mineralogy and texture. Environ. Int. 128 (December 2018), 279–291. https://doi.org/10.1016/j.envint.2019.04.022.

Eliseeva, S.V., Bünzli, J.C.G., 2011. Rare earths: Jewels for functional materials of the future. New J. Chem. 35 (6), 1165–1176. https://doi.org/10.1039/c0nj00969e.

Galunin, E., Alba, M.D., Santos, M.J., Abrão, T., Vidal, M., 2010. Lanthanide sorption on smectitic clays in presence of cement leachates. Geochim. Cosmochim. Acta 74 (3), 862–875. https://doi.org/10.1016/j.gca.2009.11.003.

Gomes, P., Valente, T., Marques, R., Prudêncio, M.I., Pamplona, J., 2022. Rare earth elements - Source and evolution in an aquatic system dominated by mine-Influenced waters. J. Environ. Manage. 322 (September) https://doi.org/10.1016/j.jenvman.2022.116125.

Gopinath, A., Divyapriya, G., Srivastava, V., Laiju, A.R., Nidheesh, P.V., Kumar, M.S., 2021. Conversion of sewage sludge into biochar: A potential resource in water and wastewater treatment. Environ. Res. 194 (May 2020), 110656 https://doi.org/10.1016/j.envres.2020.110656.

Gu, Q., Liu, J., Yang, Y., Zhu, R., Ma, L., Liang, X., Long, S., Zhu, J., He, H., 2022. The different effects of sulfate on the adsorption of REEs on kaolinite and ferrihydrite. Appl. Clay Sci. 221 (December 2021), 106468 https://doi.org/10.1016/j.clay.2022.106468.

Hadjittofi, L., Charalambous, S., Pashalidis, I., 2016. Removal of trivalent samarium from aqueous solutions by activated biochar derived from cactus fibres. J. Rare Earths 34 (1), 99–104. https://doi.org/10.1016/S1002-0721(14)60584-6.

Hartmann, E., Baeyens, B., Bradbury, M.H., Geckeis, H., Stumpf, T., 2008. A spectroscopic characterization and quantification of M(III)/clay mineral outer-sphere complexes. Environ. Sci. Tech. 42 (20), 7601–7606. https://doi.org/10.1021/es801092f.

Kołodyńska, D., Bąk, J., Majdańska, M., Fila, D., 2018. Sorption of lanthanide ions on biochar composites. J. Rare Earths 36 (11), 1212–1220. https://doi.org/10.1016/j.jre.2018.03.027.

Ladonin, D.V., 2019. Comparative Evaluation of Adsorption of Rare-Earth Elements in Some Soil Types. Eurasian Soil Sci. 52 (10), 1175–1182. https://doi.org/10.1134/S1064229319100065.

Lecomte, K.L., Sarmiento, A.M., Borrego, J., Nieto, J.M., 2017. Rare earth elements mobility processes in an AMD-affected estuary: Huelva Estuary (SW Spain). Mar. Pollut. Bull. 121 (1–2), 282–291. https://doi.org/10.1016/j.marpolbul.2017.06.030.

Li, X., Wu, P., 2017. Geochemical characteristics of dissolved rare earth elements in acid mine drainage from abandoned high-As coal mining area, southwestern China. Environ. Sci. Pollut. Res. 24 (25), 20540–20555. https://doi.org/10.1007/s11356-017-9670-5.

Liatsou, I., Pashalidis, I., Oezaslan, M., Dosche, C., 2017. Surface characterization of oxidized biochar fibers derived from Luffa Cylindrica and lanthanide binding. J. Environ. Chem. Eng. 5 (4), 4069–4074. https://doi.org/10.1016/j.jece.2017.07.040.

Migaszewski, Z.M., Gałuszka, A., Dołęgowska, S., 2019. Extreme enrichment of arsenic and rare earth elements in acid mine drainage: Case study of Wiśniówka mining area (south-central Poland). Environ. Pollut. 244, 898–906. https://doi.org/10.1016/j.envpol.2018.10.106.

Navarro, J., Zhao, F., 2014. Life-cycle assessment of the production of rare-earth elements for energy applications: A review. Front. Energy Res. 2 (NOV), 1–17. https://doi.org/10.3389/fenrg.2014.00045.

Pereira, W.V. da S., Ramos, S.J., Melo, L.C.A., Braz, A.M. de S., Dias, Y.N., Almeida, G.V. de, Fernandes, A.R., 2022. Levels and environmental risks of rare earth elements in a gold mining area in the Amazon. Environ. Res. 211 (March) https://doi.org/10.1016/j.envres.2022.113090.

Ramírez-Guinart, O., Salaberria, A., Vidal, M., Rigol, A., 2017. Assessing soil properties governing radiosamarium sorption in soils: Can trivalent lanthanides and actinides be considered as analogues? Geoderma 290, 33–39. https://doi.org/10.1016/j.geoderma.2016.12.010.

Ramírez-Guinart, O., Salaberria, A., Vidal, M., Rigol, A., 2018. Dependence of samarium-soil interaction on samarium concentration: Implications for environmental risk assessment. Environ. Pollut. 234, 439–447. https://doi.org/10.1016/j.envpol.2017.11.072.

Ramírez-Guinart, O., Kaplan, D., Rigol, A., Vidal, M., 2020. Deriving probabilistic soil distribution coefficients (K_d). Part 1: General approach to decreasing and describing variability and example using uranium K_d values. J. Environ. Radioact. 222 (April), 106362 https://doi.org/10.1016/j.jenvrad.2020.106362.

Saravanan, A., Kumar, P.S., 2022. Biochar derived carbonaceous material for various environmental applications: Systematic review. Environ. Res. 214 (P1), 113857 https://doi.org/10.1016/j.envres.2022.113857.

Serra-Ventura, J., Vidal, M., Rigol, A., 2022. Examining samarium sorption in biochars and carbon-rich materials for water remediation: batch vs. continuous-flow methods. Chemosphere 287 (P2), 132138. https://doi.org/10.1016/j.chemosphere.2021.132138.

Sheppard, S.C., 2011. Robust prediction of K_d from soil properties for environmental assessment. Hum. Ecol. Risk Assess. 17 (1), 263–279. https://doi.org/10.1080/10807039.2011.538641.

Sheppard, S., Long, J., Sanipelli, B., 2009. Solid/liquid partition coefficients (K_d) for selected soils and sediments at Forsmark and Laxemar-Simpevarp (No. SKB-R-09-27). Swedish Nuclear Fuel and Waste Management Co.

Sheppard, S., Sohlenius, G., Omberg, L.-G., Borgiel, M., Grolander, S., Nordén, S., 2011. Solid/liquid partition coefficients (K_d) and plant/soil concentration ratios (CR) for selected soils, tills and sediments at Forsmark (No. SKB-R-11-24). Swedish Nuclear Fuel and Waste Management Co.

Smith Stegen, K., 2015. Heavy rare earths, permanent magnets, and renewable energies: An imminent crisis. Energy Policy 79, 1–8. https://doi.org/10.1016/j.enpol.2014.12.015.

Sthiannopkao, S., Wong, M.H., 2013. Handling e-waste in developed and developing countries: Initiatives, practices, and consequences. Sci. Total Environ. 463–464, 1147–1153. https://doi.org/10.1016/j.scitotenv.2012.06.088.

Stumpf, T., Bauer, A., Coppin, F., Fanghänel, T., Kim, J.I., 2002. Inner-sphere, outer-sphere and ternary surface complexes: A TRLFS study of the sorption process of Eu (III) onto smectite and kaolinite. Radiochim. Acta 90 (6), 345–349. https://doi.org/10.1524/ract.2002.90.6.345.

Sun, H., Zhao, F., Zhang, M., Li, J., 2012. Behavior of rare earth elements in acid coal mine drainage in Shanxi Province, China. Environ. Earth Sci. 67 (1), 205–213. https://doi.org/10.1007/s12665-011-1497-7.

Tan, X., Liu, Y., Zeng, G., Wang, X., Hu, X., Gu, Y., Yang, Z., 2015. Application of biochar for the removal of pollutants from aqueous solutions. Chemosphere 125, 70–85. https://doi.org/10.1016/j.chemosphere.2014.12.058.

Tang, J., Johannesson, K.H., 2005. Adsorption of rare earth elements onto Carrizo sand: Experimental investigations and modeling with surface complexation. Geochim. Cosmochim. Acta 69 (22), 5247–5261. https://doi.org/10.1016/j.gca.2005.06.021.

Uddin, M.K., 2017. A review on the adsorption of heavy metals by clay minerals, with special focus on the past decade. Chem. Eng. J. 308, 438–462. https://doi.org/10.1016/j.cej.2016.09.029.

Verplanck, P.L., Nordstrom, D.K., Taylor, H.E., Kimball, B.A., 2004. Rare earth element partitioning between hydrous ferric oxides and acid mine water during iron oxidation. Appl. Geochem. 19 (8), 1339–1354. https://doi.org/10.1016/j.apgeochem.2004.01.016.

Vidal, M., Camps, M., Grebenshikova, N., Sanzharova, N., Ivanov, Y., Vandecasteele, C., Shand, C., Rigol, A., Firsakova, S., Fesenko, S., Levchuk, S., Cheshire, M., Sauras, T., Rauret, G., 2001. Soil- and plant-based countermeasures to reduce ^{137}Cs and ^{90}Sr uptake by grasses in natural meadows: The REDUP project. J. Environ. Radioact. 56 (1–2), 139–156. https://doi.org/10.1016/S0265-931X(01)00051-0.

Villar, M.V., Martín, P.L., Pelayo, M., Ruiz, B., Rivas, P., Alonso, E., Lloret, A., Pintado, X., Gens, A., Linares, J., Huertas, F., Caballero, E., Jiménez de Cisneros, C., Obis, J., Pérez, A., Velasco, V., 1998. FEBEX. Bentonite: Origin, Properties and Fabrication of Blocks. Publicación Técnica ENRESA 05/98. ENRESA, Madrid, 146 pp. ISSN 1134–380X.

Wang, Y.Y., Lu, H.H., Liu, Y.X., Yang, S.M., 2016. Ammonium citrate-modified biochar: An adsorbent for La(III) ions from aqueous solution. Colloids Surf. A: Physicochem. Eng. Asp. 509, 550–563. https://doi.org/10.1016/j.colsurfa.2016.09.060.

Yang, M., Liang, X., Ma, L., Huang, J., He, H., Zhu, J., 2019. Adsorption of REEs on kaolinite and halloysite: A link to the REE distribution on clays in the weathering crust of granite. Chem. Geol. 525 (June), 210–217. https://doi.org/10.1016/j.chemgeo.2019.07.024.

Zhao, Q., Wang, Y., Xu, Z., Yu, Z., 2021. The potential use of straw-derived biochar as the adsorbent for La(III) and Nd(III) removal in aqueous solutions. Environ. Sci. Pollut. Res. 34, 47024–47034. https://doi.org/10.1007/s11356-021-13988-2.

Zuyi, T., Xiangke, W., Xiongxin, D., Jinzhou, D., 2000. Adsorption characteristics of 47 elements on a calcareous soil, a red earth and an alumina: A multitracer study. Appl. Radiat. Isot. 52 (4), 821–829. https://doi.org/10.1016/S0969-8043(99)00262-6.